

Assessment of temperature effect in structural health monitoring with piezoelectric wafer active sensors

Tuncay Kamas^{*1}, Banibrata Poddar^{2a}, Bin Lin^{2b} and Lingyu Yu^{2c}

¹Department of Mechanical Engineering, Eskisehir Osmangazi University, Meselik Campus, 26480 Eskisehir, Turkey

²Department of Mechanical Engineering, University of South Carolina, 300 Main Str. 29208 Columbia SC, USA

(Received March 2, 2015, Revised April 29, 2015, Accepted April 30, 2015)

Abstract. This paper presents theoretical and experimental evaluation of the structural health monitoring (SHM) capability of piezoelectric wafer active sensors (PWAS) at elevated temperatures. This is important because the technologies for structural sensing and monitoring need to account for the thermal effect and compensate for it. Permanently installed PWAS transducers have been One of the extensively employed sensor technologies for in-situ continuous SHM. In this paper, the electro-mechanical impedance spectroscopy (EMIS) method has been utilized as a dynamic descriptor of PWAS behavior and as a high frequency standing wave local modal technique. Another SHM technology utilizes PWAS as far-field transient transducers to excite and detect guided waves propagating through the structure. This paper first presents how the EMIS method is used to qualify and quantify circular PWAS resonators in an increasing temperature environment up to 230 deg C. The piezoelectric material degradation with temperature was investigated and trends of variation with temperature were deduced from experimental measurements. These effects were introduced in a wave propagation simulation software called Wave Form Revealer (WFR). The thermal effects on the substrate material were also considered. Thus, the changes in the propagating guided wave signal at various temperatures could be simulated. The paper ends with summary and conclusions followed by suggestions for further work.

Keywords: PWAS; SHM; E/M impedance; WFR; thermal effects; PZT material degradation; guided wave propagation

1. Introduction

The thermal effects at elevated temperatures mostly exist for structural health monitoring (SHM) applications (Baptista *et al.* 2014, Giurgiutiu 2010, Santoni-Bottai and Giurgiutiu 2012, Xu *et al.* 2015, Yost *et al.* 2005, Kamas *et al.* 2015, Kamas 2014). The technologies for diagnosis and prognosis of SHM systems need to take the thermal effect into account and compensate it on sensing and in-situ monitoring of structures. One of the extensively employed sensor technologies

*Corresponding author, Ph.D., E-mail: tkamas@ogu.edu.tr

^a Ph.D. Student, E-mail: poddarb@email.sc.edu

^b Ph.D., E-mail: linbin@cec.sc.edu

^c Professor, E-mail: yu3@cec.sc.edu

has been permanently installed piezoelectric wafer active sensor (PWAS) for in-situ continuous SHM.

PWAS (Lin and Giurgiutiu 2010; Giurgiutiu *et al.* 2001) is light-weighted, inexpensive, unobtrusive, minimally intrusive sensor requiring low-power. PWAS is made of piezoelectric ceramic with electric field polarization, E_3 , across the electrodes deposited on both surfaces. Using the transduction of ultrasonic elastic waves into voltage and vice versa, PWAS has emerged as one of the major SHM sensing technologies and non-destructive evaluations (NDE) (Giurgiutiu *et al.* 2002, Giurgiutiu and Zagrai 2000). However, the dynamic characteristics of PWAS need to be explored prior to its installation for in-situ SHM. Electro-mechanical impedance spectroscopy (EMIS) method has been utilized as a dynamic descriptor of PWAS and as a high frequency local modal sensing technique by applying standing waves to indicate the response of the PWAS resonator by determining the resonance and anti-resonance frequencies for in-situ ultrasonics (Zagrai and Giurgiutiu 2001) such as in the work presented by Sun. (1994a, b). They utilized the EMIS method for high frequency local modal sensing.

A literature survey was first conducted to assess prior work on the survivability of PWAS at elevated temperature so that we could discover from the literature the extent of temperature dependence of the electric parameters, i.e. d_{31} and g_{31} , and the elastic parameters, i.e. s_{11} and Young's modulus (c_{11}), of different piezoelectric materials.

A NASA report by (Hooker 1998) shows the temperature dependence of d_{31} and d_{33} (Fig. 1), the effective E/M coupling coefficient as well as the thermal expansion of three different piezoelectric materials (Fig. 2).

Wolf (2004) reported increasing piezoelectric elastic compliance up to 250 K for PZT 52/48 and PZT 50/50 and their compliance values start decreasing after 250 K however other PZT material with different Zr/Ti compositions have monotonic increase until 300 K as seen in Fig. 3.

Raghavan & Cesnik reported elastic and electric properties of a piezoelectric material, PZT-5A as a function of temperature raised up to 150°C as seen in Fig. 4. The inverse of Young's modulus, Y , is the elastic compliance.

$$s = \frac{1}{Y} = \frac{\text{Strain}}{\text{Stress}} \left[\text{m}^2/\text{N}, 1/\text{Pa} \right] \quad (1)$$

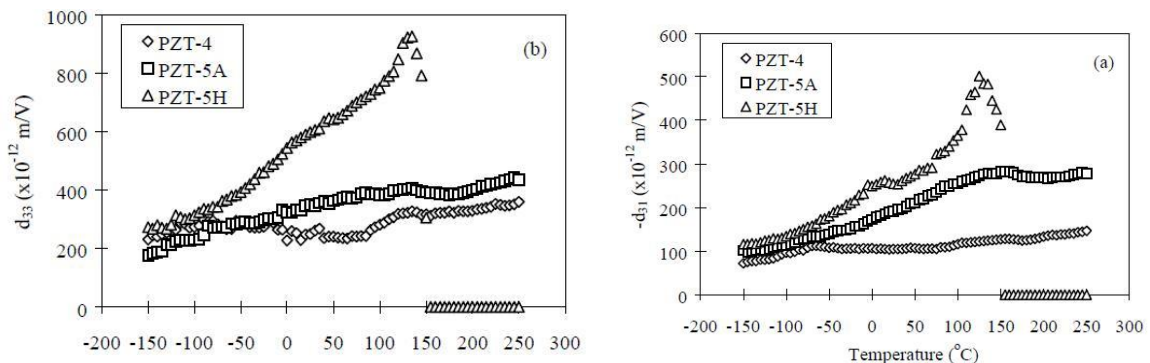


Fig. 1 $-d_{31}$ and d_{33} of three different PZT materials plotted as a function of temperature (Hooker 1998)

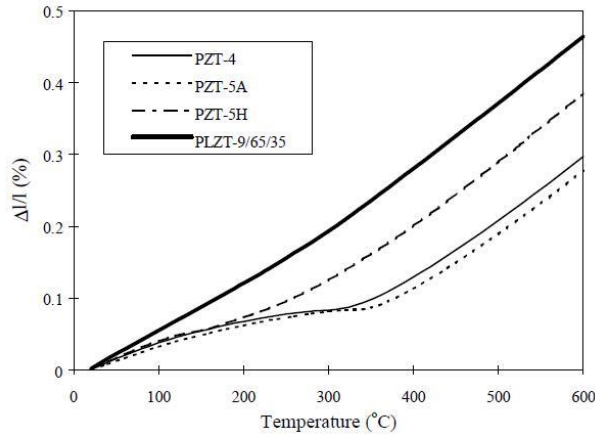


Fig. 2 Thermal expansion of three different piezoelectric materials (Hooker 1998)

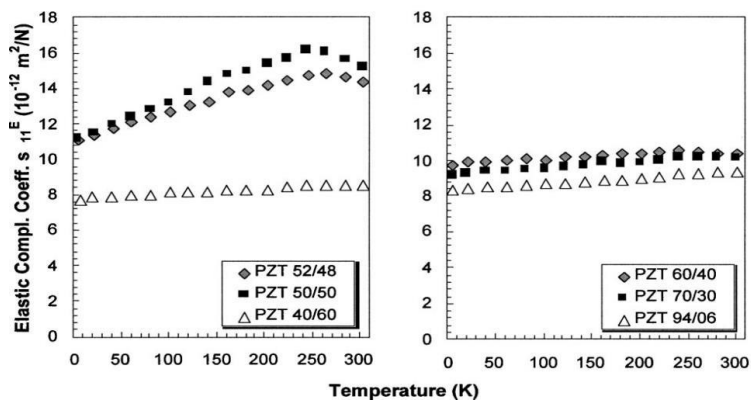


Fig. 3 Low temperature elastic compliance coefficient (s_{11}^E) plotted as a function of temperature for several tetragonal and rhombohedra PZT compositions (Wolf 2004).

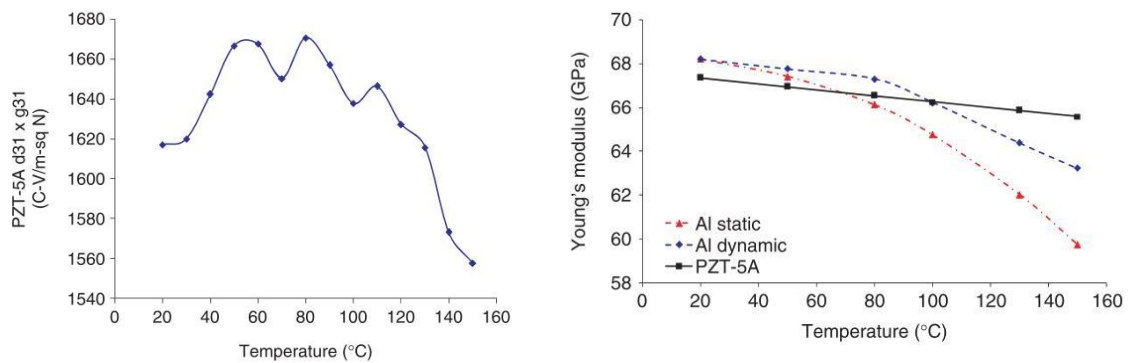


Fig. 4 Variation of Young's modulus and $d_{31} * g_{31}$. Average thermal expansion for PZT-5A; $\alpha_{PZT-5A} = 2.5 \mu\text{m/m} \cdot ^\circ\text{C}$ (Raghavan and Cesnik 2008).

Young's moduli of PZT-5A monotonically decrease as temperature increases between the room temperature and 160°C. The product of $d_{31} * g_{31}$ fluctuates along the temperature. It first monotonically inclines until 60°C, and it declines after 110°C and it goes lower than its original value at room temperature.

Wave Form Revealer (WFR) is a MATLAB GUI developed by Shen (2014) at Laboratory for Active Materials and Smart Structures (LAMSS). The purpose of this software is to simulate Lamb wave propagation in plate structures made of various materials; however this software originally was not capable of simulating temperature effects on Lamb wave propagation.

This paper presents a theoretical and experimental study of the structural health monitoring capability of PWAS at elevated temperatures. Electro-mechanical impedance spectroscopy (EMIS) method was studied using PWAS at increasing temperature. The material degradation is investigated by introducing the temperature effects on some parameters. The results from the analytical PWAS-EMIS simulations are presented. Temperature variation may produce pyroelectric charges, which may interfere with the piezoelectric effect. For the experimental validation, the EMIS measurements were conducted during temperature increase. Then, the results from the experimental cycling of PWAS at gradually increasing temperatures are discussed. Trends of the results in terms of static capacitance, C_0 , and electromechanical impedance spectroscopy (EMIS) are presented. Another goal of the paper was to develop software to simulate Lamb-wave propagation in a specimen at variable temperature. This is required to understand the variability of several different substrate material properties with temperature and how this variability effects the Lamb wave propagation in substrate structures.

2. Analytical EMIS simulations for PWAS at elevated temperatures

In this subsection, the temperature effects on free circular PWAS admittance and impedance are presented through the analytical model and the EMIS tests. The effects of the stiffness coefficient c_{11} , the piezoelectric coefficient d_{31} , and the static capacitance C_0 on impedance/admittance are taken into account.

Zagrai (2002) has developed 2-D EMIS for circular PWAS using the free circular PWAS model (Fig. 5) and the derivation procedure shown in the flow-chart in Fig. 6. In this section, we adopted herein his in-plane EMIS model to simulate the temperature effects on piezoelectric material degradation of free circular PWAS. The analytical simulation is conducted by changing the stiffness coefficient, the piezoelectric coefficient, and the capacitance. The stiffness coefficient and the piezoelectric coefficient degradation have been discussed in the literature and plots for the material properties versus temperature increase have been provided. The capacitance dependence over temperature has been defined during our experimental studies. Therefore, the proportions of the elastic and piezoelectric material property degradations are attained from the literature and the capacitance proportion was obtained from the capacitance measurements over increasing temperature. The admittance and impedance simulations are presented respectively and compared with the experimental results.

3. Experimental work

The E/M impedance is used as a direct and convenient method to implement for PWAS impedance signature as a function of temperature up to relatively high temperature, the required

equipment being an electrical impedance analyzer, such as HP 4194A impedance analyzer, PID temperature controller, and oven. The PWAS resonators tested are cylinder in diameter of 7mm and in thickness of 0.2mm. The type of piezoelectric ceramic is APC-850 whose material properties at room temperature were provided by American Piezo Company and given in Table 1.

An example of performing PWAS E/M impedance spectroscopy is presented for PWAS located in a fixture in the oven in Fig. 7. PWAS has to have stress-free i.e., unconstrained boundary conditions so that it was fixed by pogo-pins that only apply low spring forces point-wise on the PWAS surfaces in the fixture. The fixture has wires that can be connected with the probes of the EMIS analyzer instrument. The impedance analyzer reads the E/M impedance of PWAS itself in the oven. It is applied by scanning a predetermined frequency range (300 kHz-400 kHz) and recording the complex impedance spectrum. A LabVIEW data acquisition program was used to control the impedance analyzer and sweep the frequency range in steps (of 100 Hz) that was predefined and to attain the data in a format that assists to data analysis. During the visualization of the frequency sweep, the real part of the E/M impedance, $Re(Z(\omega))$, follows up and down variation as the structural impedance goes through the peaks and valleys of the structural resonances and anti-resonances.

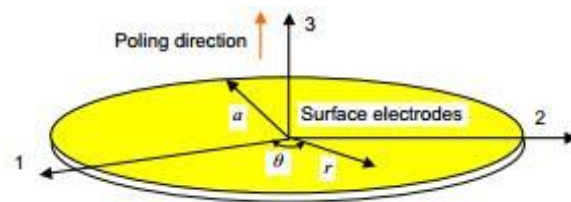


Fig. 5 Schema of circular PWAS in cylindrical coordinate system

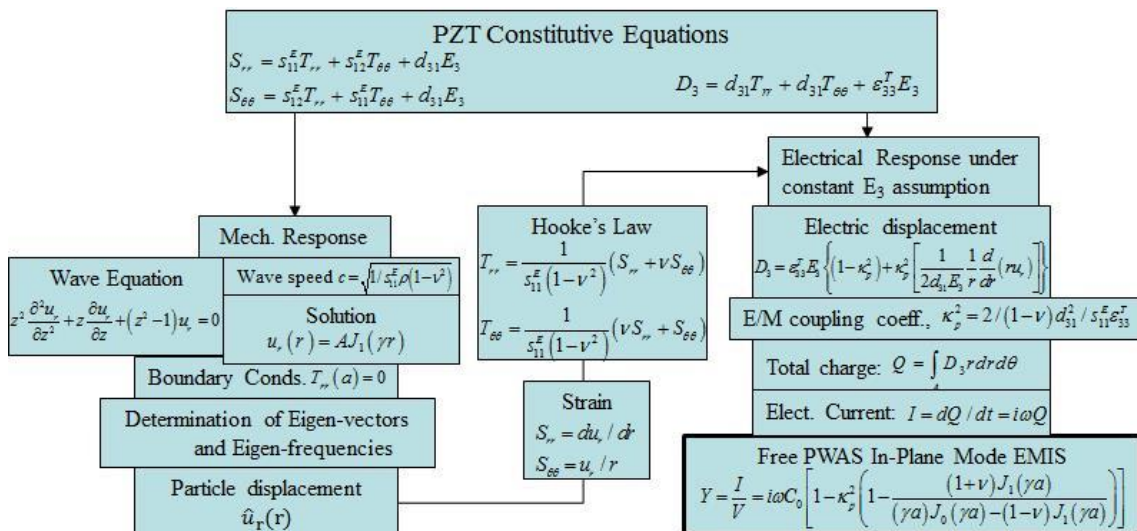


Fig. 6 Flow-chart of the analytical modeling of 2-D in-plane EMIS of circular PWAS

Table 1 Properties of APC 850 piezoelectric ceramic (www.americanpiezo.com)

Property	ρ (kg/m ³)	d_{33} (m/V)	d_{31} (m/V)	g_{33} (Vm/N)	g_{31} (Vm/N)	s_{33}^E (m ² /N)	s_{11}^E (m ² /N)	$\epsilon_{33}^T / \epsilon_0$	κ_p	κ_{33}	κ_{31}	ν
APC 850	7700	400x10 ⁻¹²	-175x10 ⁻¹²	26x10 ⁻³	-12.4x10 ⁻³	17.3 x10 ⁻¹²	15.3 x10 ⁻¹²	1750	0.63	0.72	0.36	0.35

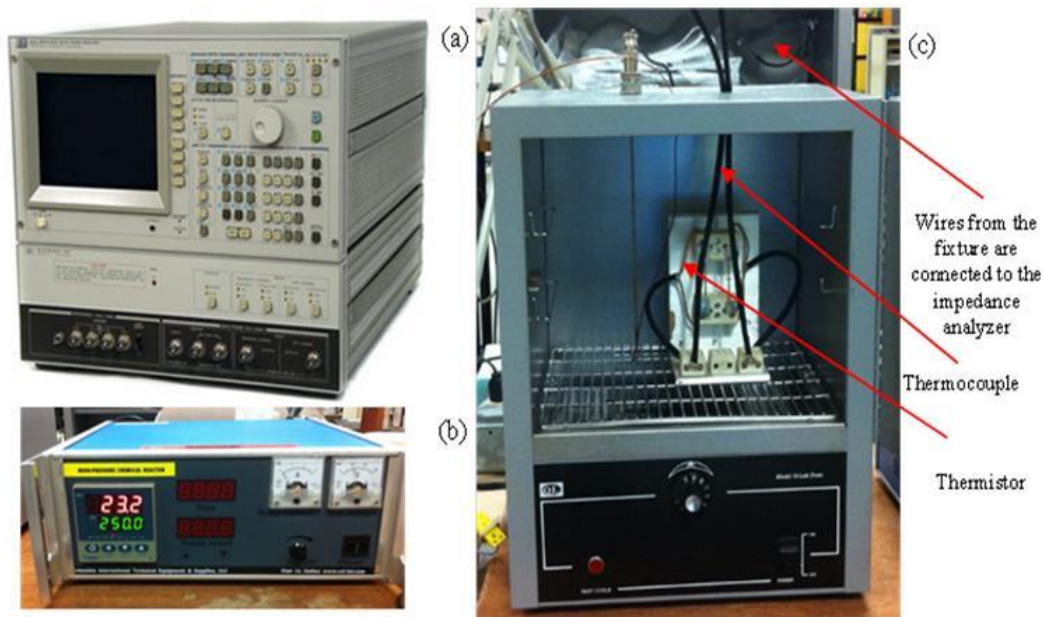


Fig. 7 High temperature PWAS testing by (a) impedance analyzer, (b) PID temperature controller and (c) oven

We aimed at observing the changes in the impedance and admittance signatures in this set of experiment. In the beginning, we conducted a set of experiments sweeping the excitation signal in the amplitude of 1 V in a wide range of frequency from 10 kHz to 1MHz to see the peaks in the spectra in in-plane modes. The first impedance peak indicated the most frequency shift due to the temperature elevation among the other in-plane peaks. Therefore, we decided to focus on the first peak. The first impedance peaks shifted down approximately from 345 kHz to 330 kHz and the first admittance peaks shifted up from 315 kHz to 325 kHz. Thus, we swept the excitation signal in the frequency range between 300 kHz and 400 kHz to observe the first admittance and impedance peaks shifting up and down respectively at elevated temperatures.

4. Results and discussion

We have measured six PWAS resonators in the elevated temperature EMIS test. We denoted them by their sequence number and a letter R or L that denotes right or left. Then PWAS 1R is the

first PWAS located on right side of the fixture and 2L is the second PWAS on the left and so on. Moreover, the first room temperature in the cycle is denoted RT1 as the second room temperature after cooling down from 50°C is denoted RT2 so that the impedance signature for the first PWAS on the right at the first room temperature is represented by 1R_RT1 and the second PWAS on the left at the third room temperature after cooling from 100°C is represented by 2L_RT3 and so on.

4.1 Capacitance results

Fig. 8 illustrates the averaged capacitance values over the static capacitance values that are obtained from six PWAS resonators. One can observe the monotonic increase in the capacitance values by increasing the temperature. The trend is linear up to 200°C; however it is interesting to see that the temperature gradient of the capacitance increases after this temperature. The capacitance values at room temperatures after each cycling also vary for the PWAS 1R.

4.2 EMIS results

We will discuss the analyses of impedance results of each PWAS in sequential subsections. We will first plot all the impedance signatures at the first in-plane anti-resonance frequency for one PWAS at all elevated temperature-room temperature cycles with a time series plot that shows each time and date when the particular measurement was performed so one can observe how long the overall measurement has taken and how long a PWAS has been kept at a certain temperature. Next, we will separate the EMIS test results as the impedance plots at room temperatures and at elevated temperatures to see the trends of the frequency and amplitude shifts of the first impedance curves in both cases. Then, we will plot the impedance amplitude vs temperature including those at room temperatures in the same graph and also plot the impedance frequency vs temperature in the same way. Finally, we will present the amplitude and the frequency shifts separately at elevated temperatures and those at room temperatures were plotted by the order number of the room temperature. The overall tests have lasted 2 days because cooling down from high temperatures to the room temperature at each cycle has taken somewhat long time. No forced convection method was implied to quicken the cooling process.

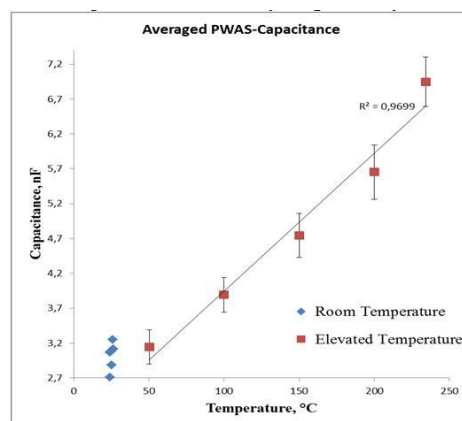


Fig. 8 Averaged static capacitance results for all of the circular PWAS resonators (Ø 7 mm x 0.2 mm) at room temperature and elevated temperatures

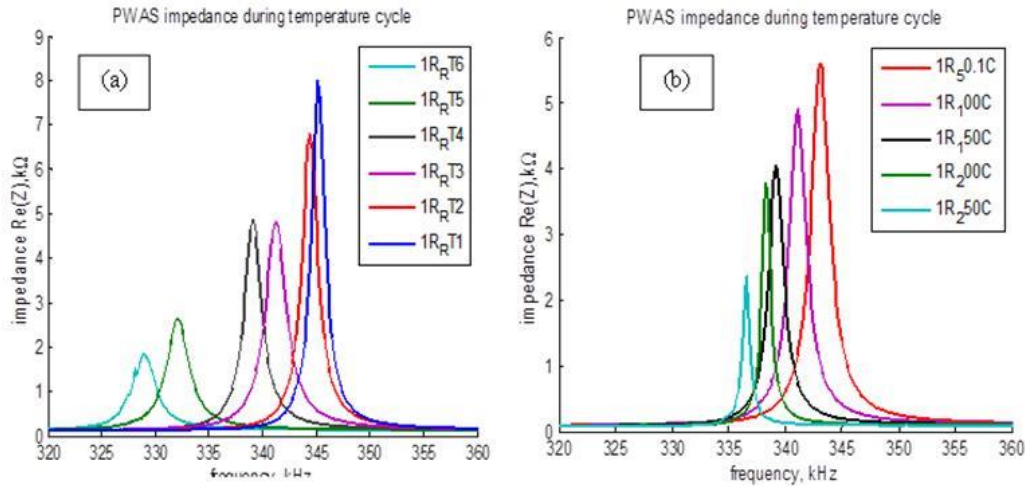


Fig. 9 Impedance signature of PWAS-1R (7 mm x 0.2 mm PWAS) at (a) elevated temperatures and (b) room temperatures in each temperature cycle

The impedance peaks diminish in amplitude as the temperature increases and it keeps diminishing even as PWAS is cooled down to the room temperature in each temperature cycle. Another phenomena is the frequency downshift as the temperature moves up however frequency upshift is also observed as PWAS cools down to the room temperature, the PWAS does not seem to recover completely and its impedance cannot move up to its original anti-resonance frequency. One interesting phenomena is also the deformation on the impedance signature of PWAS-1R at RT6 after cooling it down from 250°C as the other impedance signatures are smooth curves before.

The overall trend can be more clearly observed by examining the plots at room temperatures and the elevated temperatures separately as depicted in Fig. 9. We utilized color codes for these two plots. For instance, the impedance curve at the second room temperature ($1R_{RT2}$) has the same color as the one at the temperature of 50°C since it is the room temperature after cooling down from that temperature. The color codes are implied in such order to the other impedance curves.

In the first cycle, from the room temperature to 50°C and back to the room temperature, the impedance frequency first decreased then increased back to the close value although this does not occur in the next two cycles between the room temperature and the 100°C and the 150°C tests. In the test results from the temperature cycle between the room temperature and 100°C, the impedance frequency remains the same as the PWAS cooled down to the room temperature, which also occurs in the cycle between the room temperature and the 150°C. More significantly, in the results from the next two temperature cycles, the impedance frequency decreased even further as the PWAS cooled down back to the room temperature. The PWAS behaves in different manner after it has been heated up to 200°C due to the material degradation as the temperature approaches to the Curie temperature of the piezoelectric material and due to the depolarization that may occur.

The impedance peak amplitude and frequency against increasing temperature are plotted in Fig. 10 to analyze the trend of the amplitude and the frequency shifts over elevated temperatures.

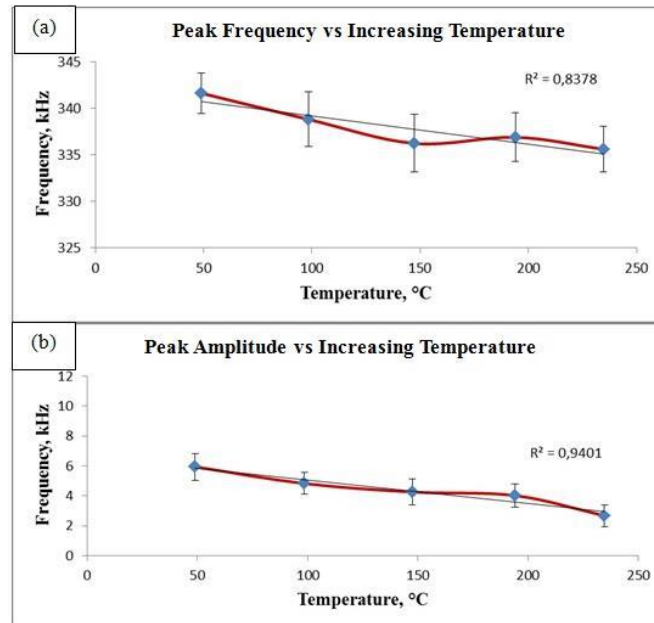


Fig. 10 Averaged impedance (a) frequency and (b) amplitude shift against elevated temperature

4.3 Comparison between analytical and the experimental EMIS results

The EMIS tests were conducted for a PWAS in an oven at elevated temperature between 50°C and 250°C with the 50°C step. During these tests, the piezoelectric material degradation was observed. The affected material properties were defined via both the literature survey and measurements. The degraded mechanical, electrical, and piezoelectric properties of PWAS were used to simulate the temperature effects on the first in-plane admittance and impedance peaks. For the analytical simulations, a 2-D circular PWAS-EMIS model was utilized. The PWAS properties used in this study are the stiffness coefficient c_{11} , the piezoelectric coefficient d_{31} , and the capacitance C_0 . The analytical and experimental results for admittance are shown in Fig. 11.

5. Experimental assessment of settling effect at elevated temperature over time

In this section, we present admittance results from free circular PWAS resonators at elevated temperatures using the same experimental setup. Temperature elevation from room temperature to higher temperatures are depicted in Fig. 12. Temperature stabilizes at constant temperature after increasing over time for each test. The PID temperature controller enables the oven settle at a certain temperature however this takes time depending upon the temperature at which it stabilizes. As observed in the temperature-time plot, the higher the temperature is, the longer time the temperatures take to settle down. In Figs. 13 and 14, counter plots of the admittance amplitude and frequency respectively over time are illustrated for the measurements conducted at different temperatures. The temperature values for the each admittance measurement were kept constant by

the closed loop temperature controller and monitored and recorded by the GUI software that was specifically designed and created for this admittance tests by Dr. Jingjing (Jack) Bao and Dr. Bin Lin of LAMSS using LabVIEW software.

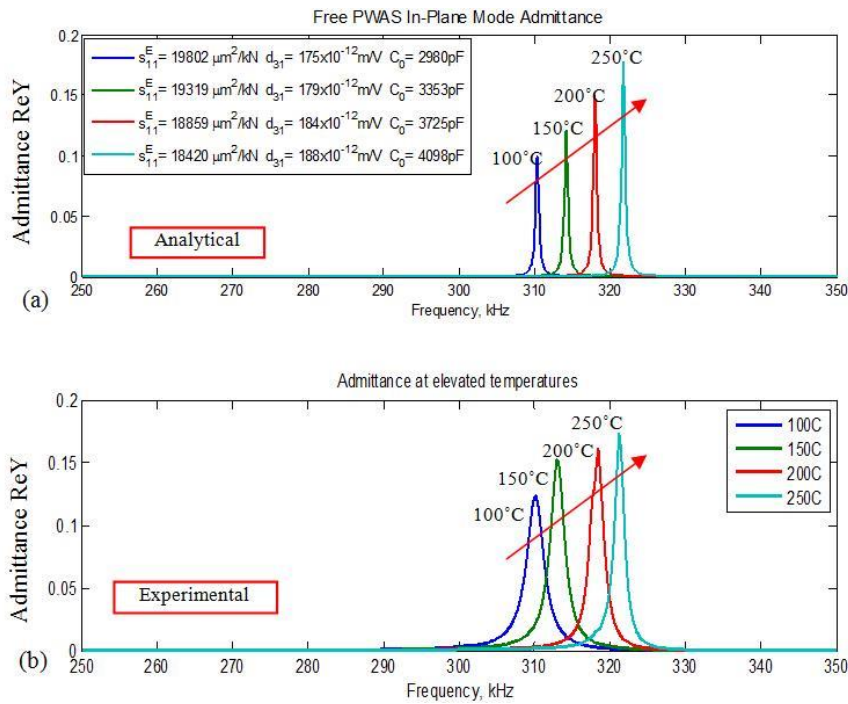


Fig. 11 Stiffness coefficient c_{11} , piezoelectric coefficient d_{31} , and capacitance C_0 influence on admittance (a) analytical prediction and (b) experimental results

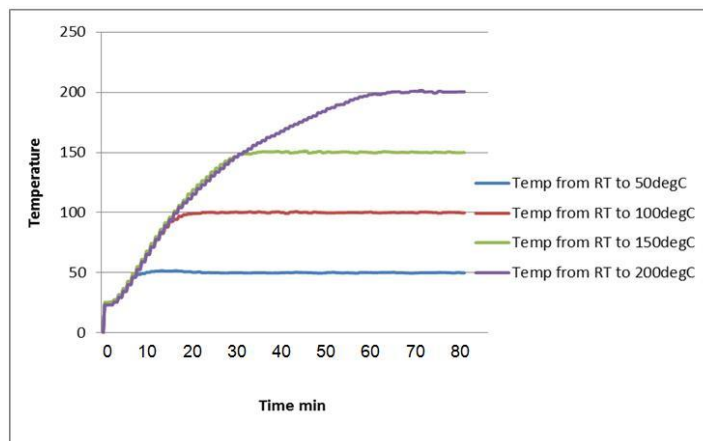


Fig. 12 Temperature stabilization over time as increasing from room temperature to 50⁰C, 100⁰C, 150⁰, and 200⁰C

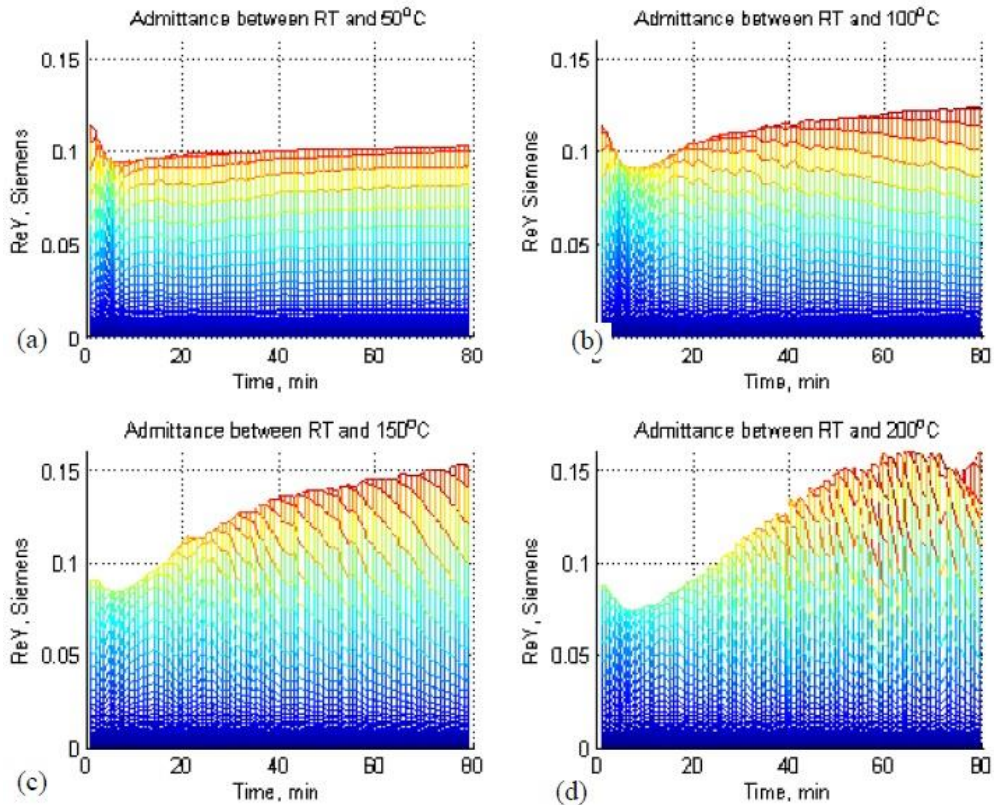


Fig. 13 Counter plots for admittance amplitude change over time at elevated temperatures: (a) up to 50°C; (b) up to 100°C, (c) up to 150°C and (d) up to 200°C.

The temperature increase from the room temperature affects the admittance amplitude and frequency settling. Since the temperature settling takes up to longer time as it increases to higher temperature, this behavior occurs at admittance amplitude and frequency. The admittance frequency was settled when the temperature stabilized by the PID temperature controller; however the admittance kept increasing over long time in order of magnitude of three days.

Admittance amplitudes from a PWAS have been measured during temperature increase from room temperature to elevated temperatures and the results were plotted and presented in Fig. 15. The admittance trend increases as the temperature increases from room temperature toward elevated temperatures. When the elevated temperature at only 50°C, the admittance amplitude was lowered to recover after return to room temperature. However, when the elevated temperatures were higher (100°C, 150°C, 200°C), the admittance amplitude did not recover completely after return to room temperature. Another interesting behavior that can be observed in this test results is that the amplitude keeps increasing with time although the elevated temperature was kept constant.

The temperature variation of the first in-plane resonance frequency values of free PWAS in an oven are plotted as in Fig. 16. The similar phenomena can be observed in the frequency shifts as it was observed in the amplitude shifts.

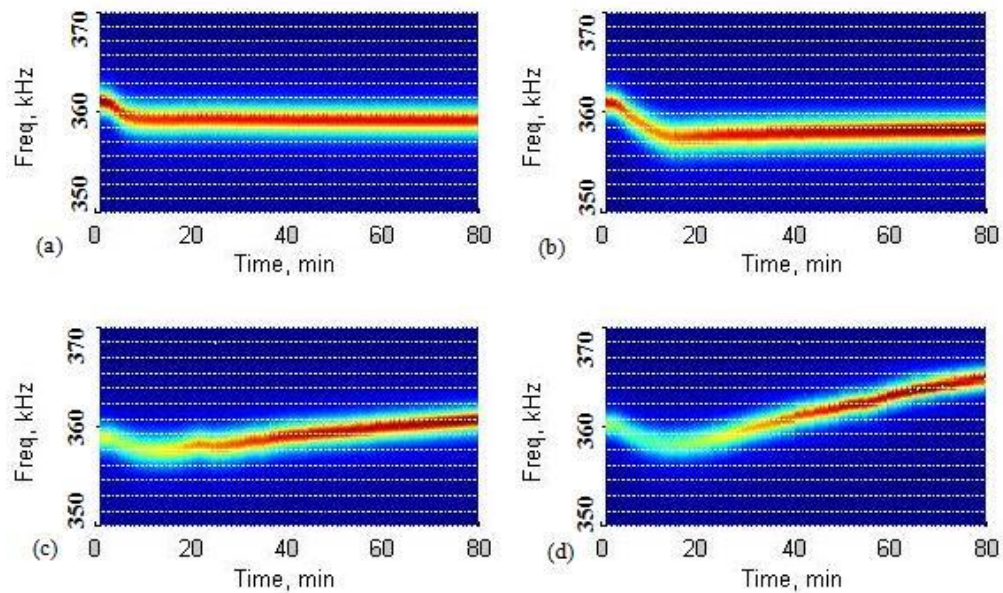


Fig. 14 Frequency-time diagram at elevated temperatures: (a) up to 50°C, (b) up to 100°C, (c) up to 150°C and (d) up to 200°C

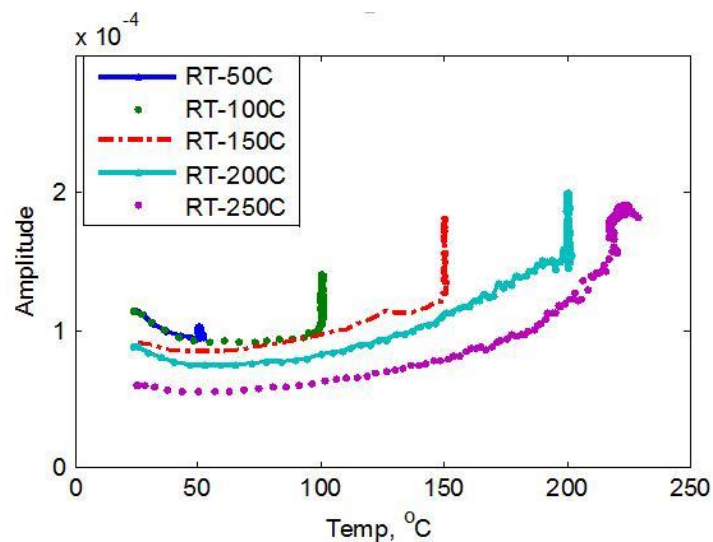


Fig. 15 Admittance peak amplitude at the first in-plane resonance frequency of circular PWAS at elevated temperatures

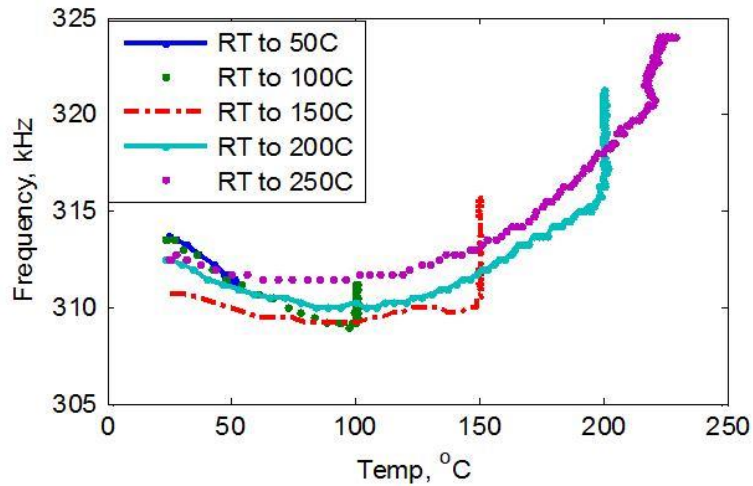


Fig. 16 Admittance frequency at the first in-plane resonance frequency of circular PWAS at elevated temperatures

6. Simulations of temperature effects on guided wave propagation

For simulating the effects of elevated temperature on the Lamb wave propagation we have changed the material properties user input of the WFR software to account for plate properties changes with temperature (Fig. 17). This was required since all the material properties of the plate depend on the temperature. Therefore, if we know the temperature, we can estimate the material properties internally within WFR using the temperature dependence of the material properties obtained from literature (Chen *et al.* 2006, Defence 1998, Hill and Shimmin 1961, Hodge and Maykuth 1968, Lees *et al.* 1924, Lipski and Mrozinski 2012, Raghavan and Cesnik 2008). WFR interpolates stored material property data to predict the material property at the user specified temperature. This allowed us to use WFR for simulating Lamb wave propagation at variable temperature.

We want to use the effect of temperature variation on each of the material properties (E , ρ , ν) separately and analyze its effect on Lamb wave propagation. Presently we used only the variation of elastic modulus with temperature to capture the effects of temperature on Lamb wave propagation. In Fig. 18, we can see the experimental data showing the variation of elastic modulus of steel 304 with temperature at specific temperatures. For a given temperature the software uses this stored data and interpolates it to get the estimated elastic modulus. This way many other material properties can be interpolated and used for Lamb wave simulation at elevated temperatures. For determining the material properties at the given temperature the software relies on stored experimental data.

Fig. 19 shows Lamb wave propagation in a steel plate simulated at two temperatures, 25°C and 200°C. We can observe a phase shift as the temperature increased. The first Lamb wave mode is the S0 wave packet and the second is the A0 mode. As seen, the phase shift in A0 wave packet is longer in comparison to that in the S0 mode.

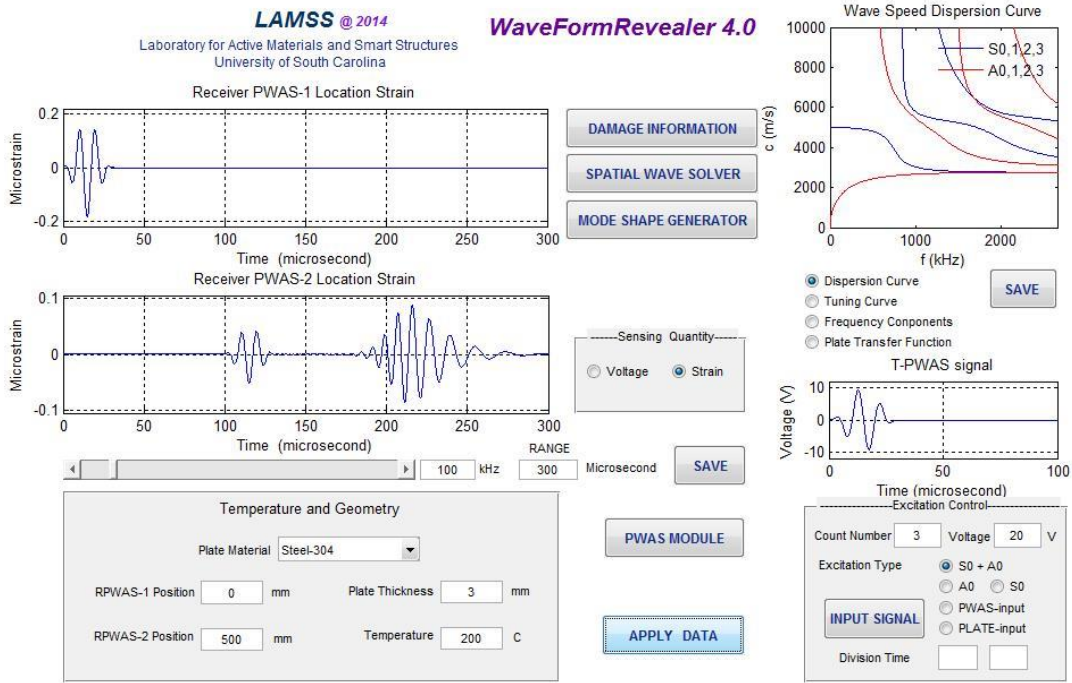


Fig. 17 Wave Form Revealer (new version)

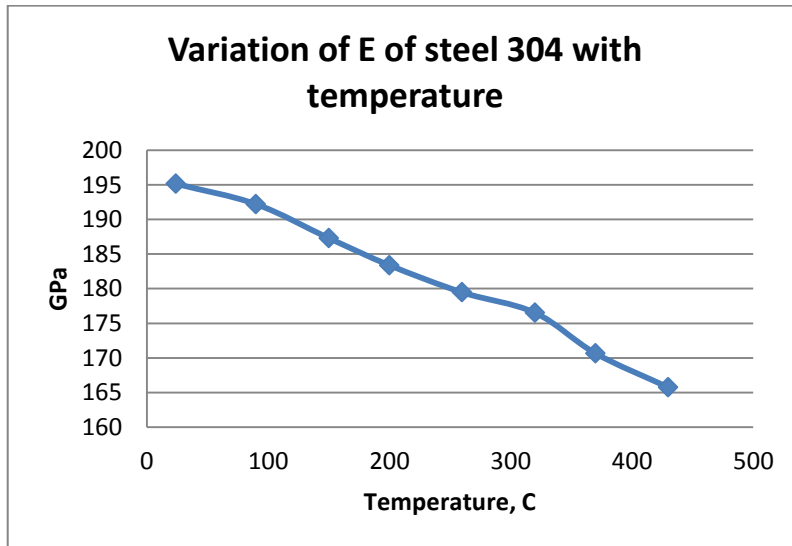


Fig. 18 Experimental data of material property (Chen *et al.* 2006)

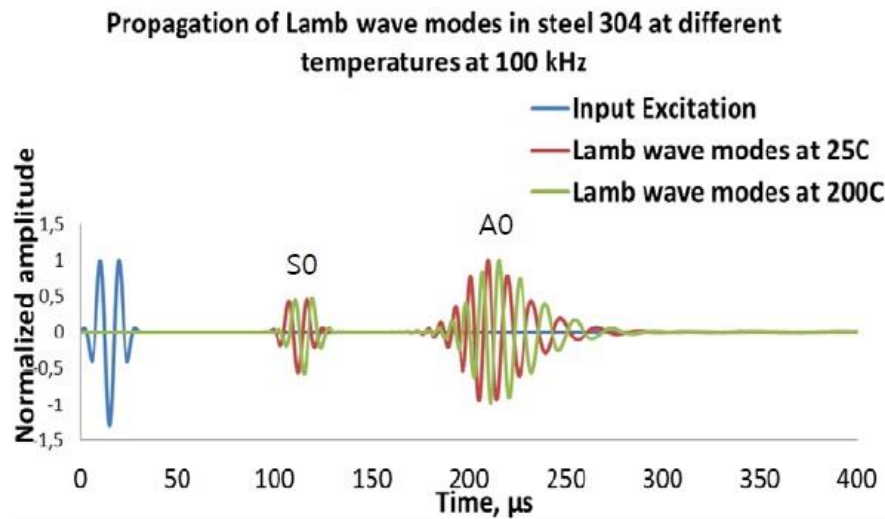


Fig. 19 Lamb wave modes simulated by modified WFR with temperature input at 25°C and 200°C

7. Conclusions

Past researches were discussed to understand the survivability of piezoelectric wafer active sensors (PWAS) at extreme environments such as at very high temperature etc. Also, we could find out the extent of temperature dependence of the electric parameters, i.e., d_{31} and g_{31} , and the elastic parameters, i.e. s_{11} and Young's modulus (c_{11}), of different piezoelectric materials.

We have conducted a preliminary parametric study to understand the effects of the material properties on the impedance (anti-resonance) and admittance (resonance) spectra of PWAS resonators. We utilized the 1-D and 2-D PWAS-EMIS models for the analytical simulations. We varied the piezoelectric stiffness and the piezoelectric charge constant by 5%. When we combined both parameter changes and simulate the impedance and admittance of PWAS, we observe both the frequency and the amplitude shifts in the plots. We have phenomenological agreement of the impedance spectra with the experimental results. However, we still need to improve the agreement by using 2-D circular PWAS-EMIS analytical model and by including more parameter changes to reflect the temperature effects on the piezoelectric material degradation. The parameter changes must be more linked to the temperature increase by using the experimental measurements in the literature. We also need to include in the model the capacitance change that was measured and found to be strongly dependent on the temperature increase.

From the experimental point of view, we observed a linear trend up to 200°C beyond which the behavior changed. In the first anti-resonance frequency peak during temperature cycle, we also observed PWAS impedance signature attempting to recover and move up in both frequency and amplitude at the room temperatures until the temperature of 200°C, it no longer recovers after 200°C which is close enough to the Curie temperature for PWAS material. The degradation of peak after 200°C is consistent with the change in capacitance behavior. Downward trend in frequency is common among PWAS-EMIS over elevated temperatures even though the shapes of trend are not consistent among samples.

Simulation of guided wave propagation with the inclusion of the thermal effects on the

substrate material was also presented. The MATLAB GUI under the name of Wave Form Revealer (WFR) was adapted for prediction of the thermal effects on coupled guided waves and dynamic structural change in the substrate material at elevated temperature. The WFR software allows for the analysis of multimodal guided waves in the structure with affected material parameters in an environment with elevated temperature.

Acknowledgments

Support from National Science Foundation Grant # CMS-0925466; and Department of Energy NEUP grant DE-NE 0000726 are thankfully acknowledged.

References

- Baptista, F.G., Budoya, D.E., De Almeida, V.A.D. and Ulson, J.A.C. (2014), "An experimental study on the effect of temperature on piezoelectric sensors for impedance-based structural health monitoring", *Sensors*, 1208-1227. <http://doi.org/10.3390/s140101208>
- Chen, J., Young, B. and Uy, B. (2006), "Behavior of high strength structural steel at elevated temperatures", *J. Struct. Eng.- ASCE*, **132**(12), 1948-1954. [http://doi.org/10.1061/\(ASCE\)0733-9445\(2006\)132:12\(1948\)](http://doi.org/10.1061/(ASCE)0733-9445(2006)132:12(1948))
- Defence, U.D. (1998), *Metallic materials and elements for aerospace vehicle structures* (Military H), USA, Department of Defence.
- Giurgiutiu, V. (2010), "Development and testing of high-temperature piezoelectric wafer active sensors for extreme environments", *Struct. Health Monit.*, **9**(6), 513-525. <http://doi.org/10.1177/1475921710365389>
- Giurgiutiu, V., Bao, J. and Zhao, W. (2001), "Active sensor wave propagation health monitoring of beam and plate structures", *Proceedings of the SPIE's 8th International Symposium on Smart Structures and Materials*. Newport Beach, CA.
- Giurgiutiu, V., Zagrai, A. and Jing Bao, J. (2002), "Piezoelectric wafer embedded active sensors for aging aircraft structural health monitoring", *Struct. Health Monit.*, **1**(1), 41-61. <http://doi.org/10.1177/147592170200100104>
- Giurgiutiu, V. and Zagrai, A. (2000), "Damage detection in simulated aging-aircraft panels using the electro-mechanical impedance technique", *Proceedings of the Adaptive Structures and Material Systems Symposium, ASME Winter Annual Meeting*, Orlando, FL.
- Hill, W.H. and Shimmin, K.D. (1961), *Elevated temperature dynamic elastic moduli of various metallic materials*.
- Hodge, A.W. and Maykuth, D.J. (1968), Properties of new high temperature Titanium alloys, DMIC Memo.
- Hooker, M.W. (1998), *Properties of PZT-Based Piezoelectric Ceramics Between – 150 and 250 C*. Hampton, Virginia.
- Kamas, T. (2014), *Behavior of Piezoelectric Wafer Active Sensor in Various Media*. University of South Carolina.
- Kamas, T., Frankforter, E., Lin, B., Yu, L. and Giurgiutiu, V. (2015). "Thermal effect on E/M impedance spectroscopy of piezoelectric wafer active sensors", *Proceedings of thSPIE 2015 Smart Structure/NDE*, San Diego, CA.
- Lees, C.H., Andrews, P. and Shave, L.S. (1924), "The variation of Young's modulus at high temperatures", *Proceedings of the Physc. Soc.*, London.
- Liang, C., Sun, F.P. and Rogers, C.A. (1994), "Coupled electro-mechanical analysis of adaptive material systems -- determination of the actuator power consumption and system energy transfer", *J. Intel. Mat. Sys. Str.*, **5**(1), 12-20. <http://doi.org/10.1177/1045389X9400500102>
- Lin, B. and Giurgiutiu, V. (2010), "Modeling of power and energy transduction of embedded piezoelectric

- wafer active sensors for structural health monitoring”, **7981**, 76472P-76472P-12. <http://doi.org/10.1117/12.880120>
- Lipski, A. and Mrozinski, S. (2012), “The effects of temperature on the strength properties of aluminum alloy 2024-T3”, *Acta Mech. Autom.*, **6**(3), 62-66.
- Raghavan, A. and Cesnik, C.E.S. (2008), “Effects of elevated temperature on guided-wave structural health monitoring”, *J. Intel. Mat. Syst. Str.*, **19**(12), 1383-1398. <http://doi.org/10.1177/1045389X07086691>
- Santoni-Bottai, G. and Giurgiutiu, V. (2012), “Damage detection at cryogenic temperatures in composites using piezoelectric wafer active sensors”, *Struct. Health Monit.*, **11**(5), 510-525. <http://doi.org/10.1177/1475921712442441>
- Shen, Y. (2014), *Structural Health Monitoring Using Linear and Nonlinear Ultrasonic Guided Waves*. University of South Carolina.
- Sun, F.P., Liang, C. and Rogers, C.A. (1994), “Structural modal analysis using collocated piezoelectric actuator/sensors: an electromechanical approach”, *Proceedings of the SPIE 2190, Smart Structures and Materials 1994: Smart Structures and Intelligent Systems*, Orlando, FL.
- Wolf, R.A. (2004), “Temperature dependence of the piezoelectric response in lead zirconate titanate films”, *J. Appl. Phys.*, **95**(3), 1397. <http://doi.org/10.1063/1.1636530>
- Xu, D., Banerjee, S., Wang, Y., Huang, S. and Cheng, X. (2015), “Temperature and loading effects of embedded smart piezoelectric sensor for health monitoring of concrete structures”, *Constr. Build. Mater.*, **76**, 187-193. <http://doi.org/10.1016/j.conbuildmat.2014.11.067>
- Yost, W. T., Macias, B.R., Cao, P., Hargens, A.R. and Ueno, T. (2005), “System for determination of ultrasonic wave speeds and their temperature dependence in liquids and in vitro tissues”, *J. Acoust. Soc. Am.*, Retrieved from <http://www.ncbi.nlm.nih.gov/pubmed/15759685>
- Zagrai, A.N. (2002), *Piezoelectric wafer active sensor electro-mechanical impedance structural health monitoring*, University of South Carolina, Retrieved from <http://onlinelibrary.wiley.com/doi/10.1002/cbdv.200490137/abstract>
- Zagrai, A.N. and Giurgiutiu, V. (2001), Electro-Mechanical Impedance Method for Damage Identification in Circular Plates, 40.